Electronic Supplementary Information

Boron based nanosheets as reducing templates in aqueous solutions: Towards novel nanohybrids with gold nanoparticles and graphene

Asha Liza James,[a] Shikha Khandelwal,[b] Arnab Dutta[b] and Kabeer Jasuja*[a]

[a]Discipline of Chemical Engineering,
Indian Institute of Technology Gandhinagar, Gujarat 382355, India.
Email: kabeer@iitgn.ac.in

[b]Discipline of Chemistry,
Indian Institute of Technology Gandhinagar, Gujarat 382355, India.
Email: arnab.dutta@iitgn.ac.in.

S1: Experimental Section

Materials:

Magnesium diboride powder (-100 mesh size, 99% purity), ethylene diamine tetraacetic acid disodium salt dihydrate (> 98.5%), *p*-benzoquinone (≥98%), gold (III) chloride trihydrate (≥99.9% trace metals basis), silver nitrate (≥99.9%) and phosphate buffer solution (1.0 M, pH 7.4) were purchased from Sigma-Aldrich. Chloroplatinic acid hexahydrate was purchased from Rankem Reagents. Anthraquinone (97% purity), 3,5-di-tert-butyl-*o*-benzoquinone (98% purity), 9,10-phenanthraquinone (≥ 99% purity), benzil (98% purity), deuterium oxide (99.9 atom % D) dimethyl sulfoxide-d_6 (99.9 atom% D) and Nafion perfluorinated resin solution (5 wt. % in lower aliphatic alcohols and water, contains 15-20% water) were purchased from Aldrich and used as received without further purification. Potassium permanganate (assay >98.5%) and sulphuric acid (assay 95-98%) were purchased from Merck. Graphite powder (100 microns), sodium nitrate (minimum assay 99.5%), and hydrogen peroxide (30% w/v) were from SDFCL. Hydrochloric acid (assay 35.8-38%) was from Fisher Scientific. Sodium sulphate anhydrous (AR grade) was purchased from Finar Chemicals Private Ltd, Millipore Ultrapure Type I water (resistivity of 18.2 MΩ.cm at 25ºC) was used as deionized (DI) water in all experiments. Snakeskin dialysis tubings (10 kDa MWCO, 35 mm diameter, Thermofisher) were used for dialysis of the nanosheet dispersions.

Characterization:

Transmission electron microscopic imaging was performed using a Philips Tecnai 20 TEM, operated at 200 kV. The nanomaterial dispersion was deposited onto lacey carbon copper grids (Ted Pella, 300 mesh) and dried under ambient conditions before imaging. High-resolution TEM, STEM, and EELS experiments were performed on a JEOL JEM 2200 FS Field Emission Electron Microscope. JEOL JSM-7600F operated at 5 kV was used for field emission scanning electron microscopy (FE-SEM). AFM imaging was performed on a Bruker Multimode-8-AM in ScanAsyst tapping mode. Samples for AFM were prepared by re-dispersing the lyophilized powder in DI water and spin coating ~20 µl of this dispersion (at 3000 rpm, for 60 seconds) onto freshly cleaved mica substrate (10 mm, Ted Pella).

UV-Vis spectroscopy was performed on a Perkin Elmer Lambda 365 UV-Vis spectrophotometer using 10 mm path length quartz cuvettes. ICP-AES studies were carried out on a Perkin Elmer ICP-OES Spectrometer Optima 3300 RL; the nanomaterial samples were analyzed against Ultrapure Millipore water (Type I) as the control. FTIR spectra were recorded on a Perkin Elmer Spectrum Two spectrometer equipped with ATR accessory. Solid state ^{11}B NMR spectra were recorded on an ECX-II-JEOL 400MHz instrument with a 9.4 T magnet, equipped with a 4 mm magic angle spinning (MAS) probe operated at 10

kHz. Solution based ^{1}H NMR spectra were recorded on a Bruker Avance III 500 MHz spectrometer. X-ray photoelectron spectroscopy was performed on Axis Ultra, Kratos Analytical, Shimadzu with monochromatic Al Kα X-ray with hν of 1486.6 eV. Raman spectra were recorded using 785 nm laser by Renishaw inVia confocal Raman microscope.

Synthesis of boron based nanosheets:

The boron based nanosheets were prepared according to a recipe modified from a previous report.[1] Briefly, 1.15 g magnesium diboride (MgB_2) powder was mixed with 250 ml of 0.1M disodium EDTA solution and magnetically stirred at 300 rpm for one hour, with the temperature maintained at ~22 ºC. The solution was left to settle for a day, after which the clear top part was recovered by two rounds of centrifugation at 3000 rpm. The final supernatant was dialyzed against DI water (to remove residual salts and ionic species) for ~40 hours to obtain a transparent colloidal dispersion of nanosheets, which was stored at 4 ºC before further use. The dialyzed samples were subjected to lyophilization for ~48 hours to obtain the powder-form of these nanosheets.

Test for reducing action with $KMnO_4$:

A stock solution of 0.01 M $KMnO_4$ was prepared and suitably diluted for further experiments. To 2 ml of 0.001 M $KMnO_4$ solution, 1 ml colorless nanosheet dispersion (~0.5 mg/ml) was mixed, and then the reaction was monitored by UV Vis spectroscopy. The nanosheets' action on $KMnO_4$ solution was temporally monitored as a decrease in the characteristic absorbance peaks in the region ~460-600 nm. The fall in absorbance of the most prominent peak at ~525 nm was plotted with time and fitted to first order reaction kinetics as shown in Figure S1. The change in color of the sample has also been captured in the Movie S1. A control experiment was carried out by reducing $KMnO_4$ with $NaBH_4$: 2 ml of 0.001 M $KMnO_4$ was mixed with 1 ml of 0.001 M $NaBH_4$ and the reaction was monitored by UV-Vis spectroscopy. This reaction has been depicted in the Movie S2.

Test for reducing action with organic molecules:

A 1 mM stock solution of *p*-benzoquinone was made in water. To 0.2 ml of this solution, 1 ml of the aqueous dispersion of nanosheets (0.5 mg/ml) was added, and the sample was made up to 3 ml using DI water. This reaction was monitored by UV-Vis spectroscopy for the temporal variation in its absorbance spectrum. For conducting ^{1}H solution NMR studies, a 1 mM solution of *p*-benzoquinone was made in D_2O, and its NMR spectrum was recorded. Lyophilized powder-form of nanosheets (2.4 mg) was dispersed in 150 µl of D_2O. Then, 50 µl of the nanosheets dispersion was mixed with 600 µl of the *p*-

benzoquinone solution, and the reaction was monitored with time by recording the NMR spectrum periodically.

These NMR studies were repeated for the following organic molecules: 3,5-di-tert-butyl-*o*-benzoquinone, anthraquinone, 9,10-phenanthraquinone, and benzil. While these compounds were dissolved in DMSO-d_6 for all experiments, the nanosheets dispersions were made in D_2O. Control experiments were performed for the reduction of all the above organic molecules with $NaBH_4$ as per the following procedure. 50 µl of $NaBH_4$ solution (10 mM) was mixed with 600 µl of 1 mM solution of the respective organic compound in DMSO-d_6. The ^1H NMR spectra of the compounds were recorded before and after addition of $NaBH_4$.

Synthesis of AuNP decorated nanosheets:

To 10 ml aqueous dispersion of nanosheets being vigorously stirred at 500 rpm, 100 µl of 0.01 M gold salt (gold (III) chloride trihydrate) solution was added drop by drop. An immediate color change to reddish brown was observed as soon as the yellow gold salt solution mixed with the colorless nanosheet dispersion. This has been captured in the Movie S3. The solution was left stirring for one hour at ambient conditions (temperature of ~25ºC). The hence formed nano-hybrids dispersions are stored at 4ºC until further use.

A similar protocol was followed for the reduction of silver nitrate and chloroplatinic acid as well, wherein dark yellow colored and black colored dispersions formed respectively.

Synthesis of graphene oxide nanosheets:

Graphene oxide was synthesized as per the protocol reported by Compton et al.[2] To a 500 ml round bottom flask, 28.75 ml sulfuric acid was added. To the acid, 1.25 g graphite powder and 0.625 g sodium nitrate were added, and the sample was mixed in an ice bath for ~10 minutes. To the dark black suspension, potassium permanganate was added slowly, upon which the color changed to dark green. This mixture was then transferred to a water bath maintained at 35 ºC and vigorously stirred for 3 hours. The resulting dark brown, viscous liquid was cooled on ice and 57.5 ml deionized water was added slowly to it. Then, the sample was suspended in 230 ml deionized water and 3 ml hydrogen peroxide was added for quenching. The as-synthesized graphite oxide was washed and purified by three cycles of centrifugation in acid and water. The suspension was centrifuged (8230g, 5 min), the supernatant decanted, the dark-coloured sediments re-suspended in 4% HCl, and then centrifuged again. After three rounds of washing in acid, the procedure was repeated with deionized water. The purified graphite oxide thus obtained was re-suspended in 125 ml deionized water and then subjected to ultrasonication (30% amplitude, 10 seconds ON/ 10 seconds OFF pulse) for a total time of one hour sonic ON. The sonicated suspension was then

centrifuged at 8230 g for five minutes to let any unexfoliated graphite oxide sediment. The top part was collected as the exfoliated graphene oxide suspension. In order to remove the residual salts, the graphene oxide dispersion was dialyzed against deionized water for 48 hours.

Reduction of graphene oxide by the boron based nanosheets:

Aqueous graphene oxide dispersion of concentration 0.5 mg/ml was used in all experiments. To 1.5 ml of the above solution which appeared yellowish brown, 3.5 ml of clear aqueous boron based nanosheet dispersion was added and stirred for 2 hours. After two hours, the sample was left undisturbed at ambient conditions. After 12 hours, the sample exhibited two phases - a black precipitate settled at the bottom and a top clear supernatant.

Electrochemistry experiments

Electrocatalytic measurements were performed using a Metrohm Autolab PGSTAT 101 potentiostat with a three-electrode setup. The experiments were carried out in a phosphate buffer solution of pH 7.4, at room temperature, and under nitrogen atmosphere. A 3mm glassy carbon electrode, coated with the nanomaterial, was used as the working electrode along with a Pt-wire counter electrode and Ag/AgCl (in saturated KCl) as the reference electrode.

The coating of nanomaterial on the working electrodes was obtained by drop-casting the respective dispersions, as follows: The powder form of the nanomaterials was mixed with DI water, ethanol, and Nafion (5 wt%) (v/v/v = 4/1/0.02) to form a 2 mg/ml dispersion under sonication. 10 µl of the above dispersion was deposited onto the 3 mm glassy carbon working electrode and dried in a vacuum desiccator for 12 hours.

All the potential values of the cyclic voltammetry data were internally referenced against $Fe(CN)6^{3-/4-}$ couple ($E_{1/2}$ = +0.36 V vs SHE) and calibrated against SHE. Anhydrous sodium sulphate was used as a supporting electrolyte during the experiment. After each run, the glassy carbon electrode was polished using a slurry of 0.05 µm alumina powder in deionized water.

S2: Supporting Results

S2.1. Elucidating the reducing properties of boron based nanosheets

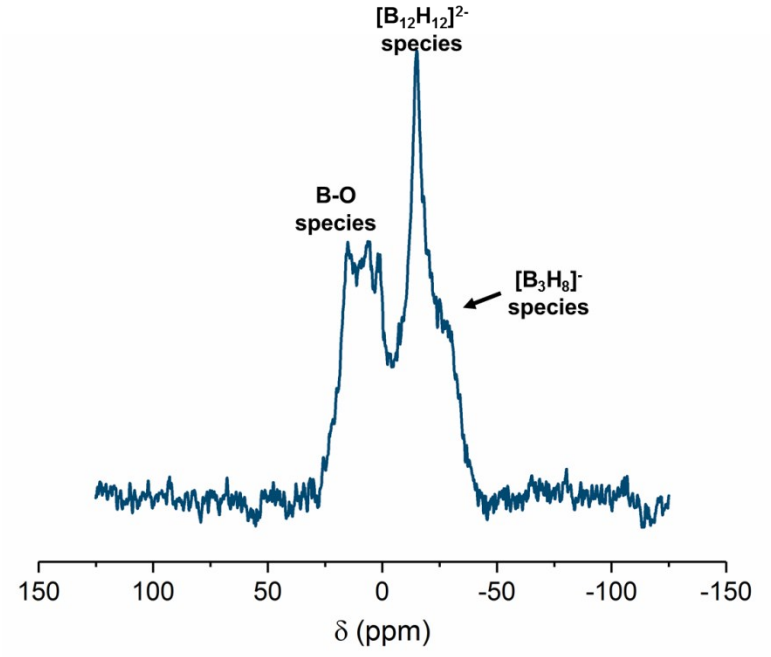

Figure S1: Solid state ^{11}B NMR spectrum of the boron based nanosheets chemically exfoliated from layered MgB_2 showing the presence of complex borohydride (B_xH_y) groups and oxy groups.

Upon chelation assisted exfoliation of layered MgB_2 in water, the resultant boron based nanosheets are found to acquire functional groups derived from the aqueous environment. The gain of functional groups can be attributed to two main factors:

i. The partial loss of Mg atoms between the boron layers (due to sequestration by the chelating agent) is compensated by gaining oxy, hydroxyl, and hydride groups onto the boron planes from the surrounding aqueous milieu.[1]
ii. Bulk MgB_2 is known to undergo reaction with water and release gaseous boranes, leading to its surface degradation.[3,4] Such reactions could also occur in water during exfoliation because the available surface area is much higher at the nanoscale.

The solid-state NMR data indicates the presence of complex borohydride groups on the nanosheets. Upon comparing with the available literature, we could identify that the peak near -15 ppm corresponds to $[B_{12}H_{12}]^{2-}$and the shoulder peak around -28 ppm corresponds to $[B_3H_8]^{2-}$.[5]

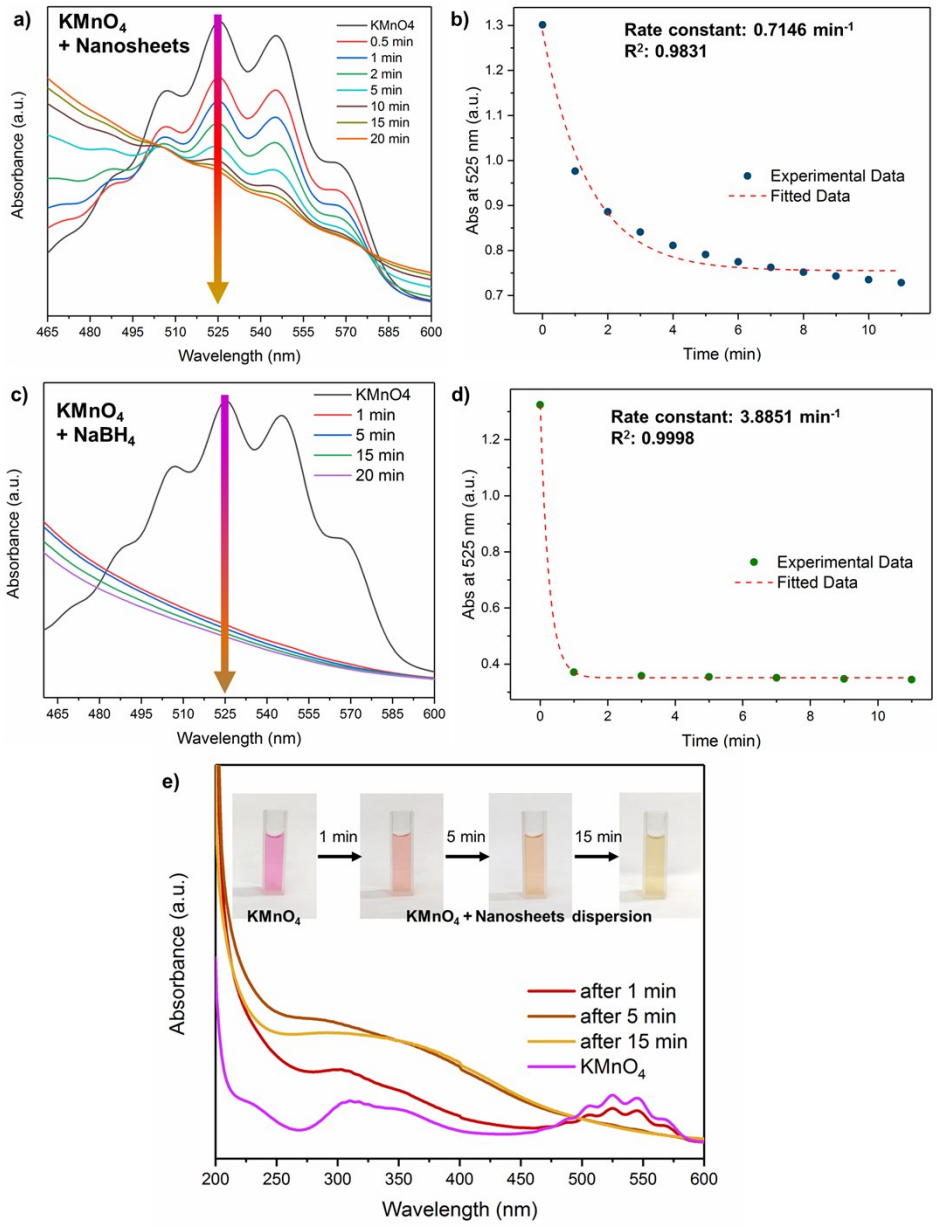

Figure S2: Monitoring the reduction of $KMnO_4$ by UV-Vis spectroscopy: (a) Upon addition of boron based nanosheets, the $KMnO_4$ solution exhibited a gradual decrease in the intensity of its characteristic absorbance peaks; (b) The fall in the intensity of absorbance measured at 525 nm as a result of reduction elicited by the boron based nanosheets was found to follow a first-order reaction kinetics with a rate constant of 0.7146 min^{-1}; (c) On the other hand, upon adding $NaBH_4$ to $KMnO_4$, a rapid fall in absorbance is observed; (d) The fall in absorbance at 525 nm was also fitted to first order kinetics with a rate constant of 3.8851 min^{-1}, which is ~5 times higher than that in the case of reduction with nanosheets; (e) Photographs and full range UV-Vis spectra showing the time-dependent change in colour upon adding the nanosheets: purple coloured $KMnO_4$ changes to reddish orange to brown and then gradually turned

yellow. This is likely due to the stepwise reduction of Mn(VII) to Mn(VI) to Mn(V) and eventually to Mn(IV) wherein the MnO_2 precipitates (Fig. 1c in the main file). Such stepwise reduction steps are not discernible when $KMnO_4$ is reduced by $NaBH_4$ (Movie S1 and Movie S2).

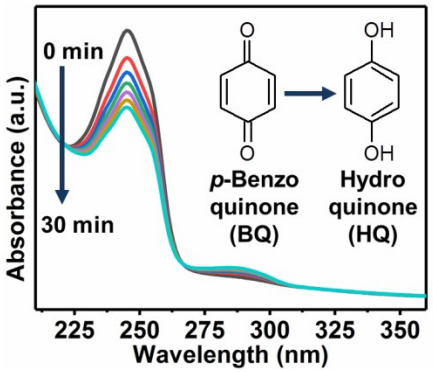

Figure S3: Monitoring the reduction of p-benzoquinone by UV Vis spectroscopy: The peak at ~245 nm corresponding to p-benzoquinone is found to fall with time with a subsequent slight increase in the peak ~287 nm.

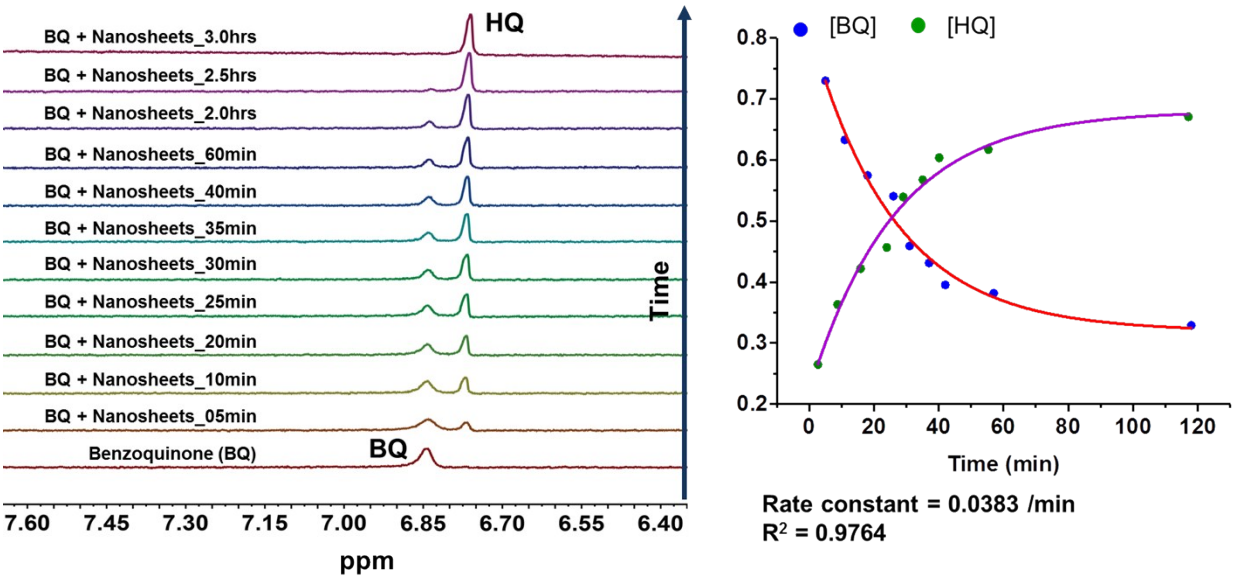

Figure S4: Monitoring the reduction of p-benzoquinone by ^1H solution NMR spectroscopy: (a) A solution of p-Benzoquinone and boron based nanosheets exhibits a gradual fall in the peak at ~6.85 ppm (which corresponds to benzoquinone BQ) and an associated rise in the peak at ~6.75 ppm (which corresponds to hydroquinone HQ), as monitored by ^1H solution NMR spectroscopy; (b) Experimental and fitted kinetic data for the conversion of BQ into HQ over two hours are also presented, indicating a rate constant of ~0.038 min^{-1}.

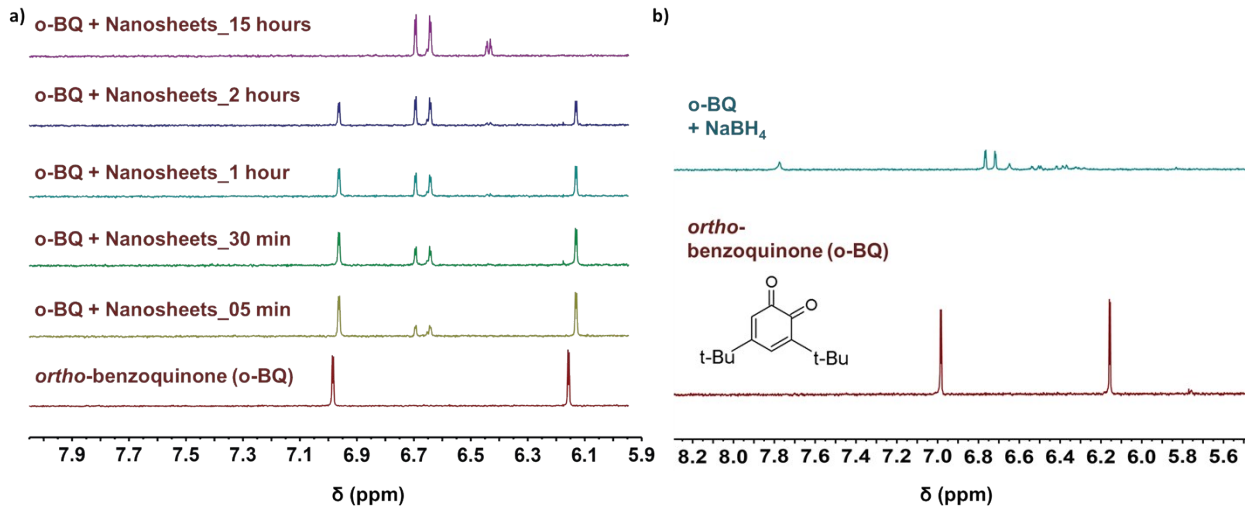

Figure S5: Monitoring the reducing effect of (a) boron based nanosheets and (b) $NaBH_4$ on 3,5-di-tert-butyl-o-benzoquinone by ^1H solution NMR spectroscopy. The nanosheets reduce the compound gradually over a period of few hours while $NaBH_4$ immediately reduces the compound upon mixing.

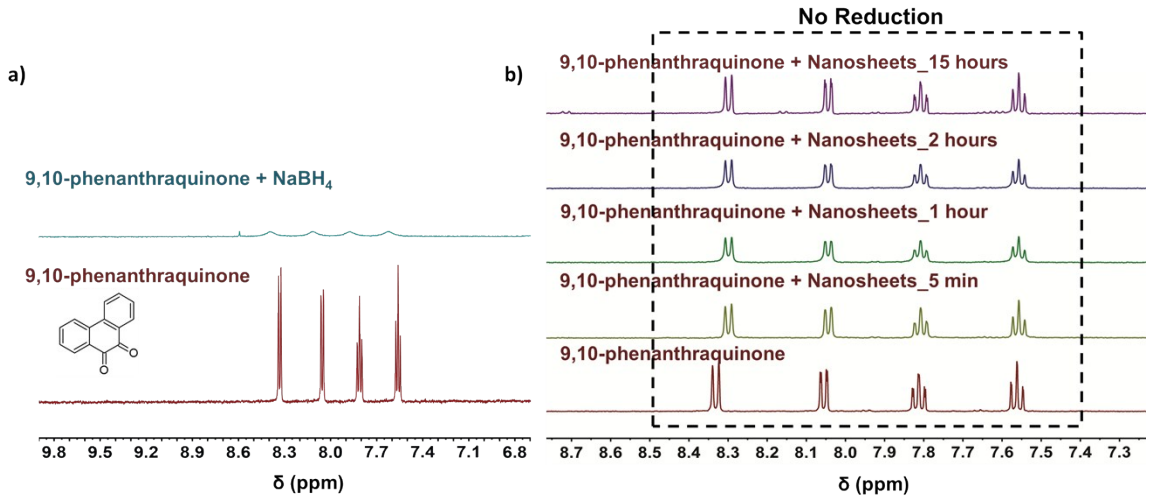

Figure S6: (a) Monitoring the $NaBH_4$ mediated reduction of 9,10-phenanthraquinone by ^1H solution NMR spectroscopy wherein the compound is immediately reduced upon mixing; (b) Upon adding nanosheets to 9,10-phenanthraquinone, there is no change in the compound's ^1H NMR spectrum, indicating that the compound could not be reduced by the nanosheets, even after 15 hours of interaction.

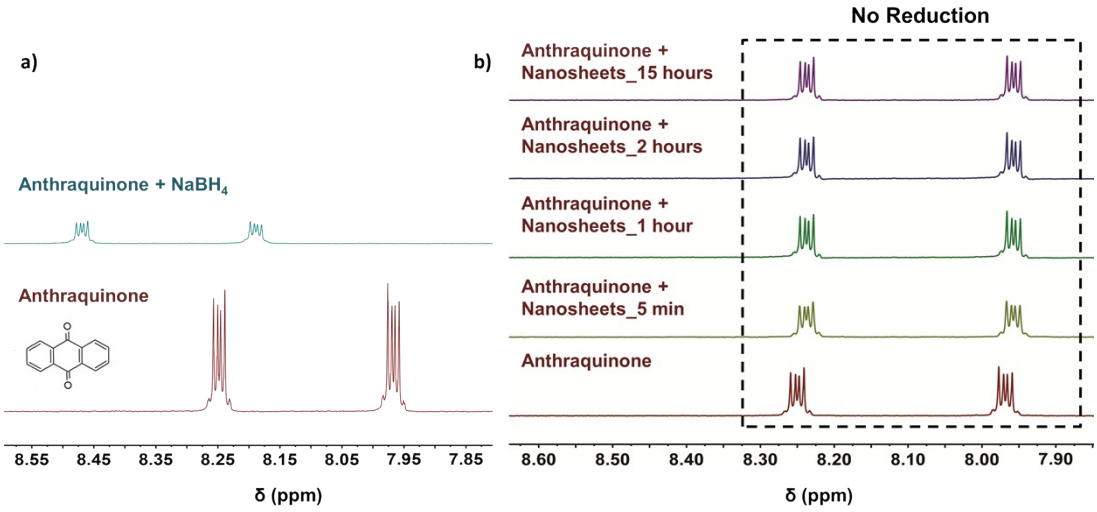

Figure S7: (a) Monitoring the $NaBH_4$ mediated reduction of anthraquinone by ^1H solution NMR spectroscopy wherein the compound is immediately acted on by $NaBH_4$ upon mixing; (b) Adding the nanosheets to anthraquinone does not result in any change in the compound's ^1H NMR spectrum, indicating that the nanosheets are unable to reduce the compound, even after 15 hours of interaction.

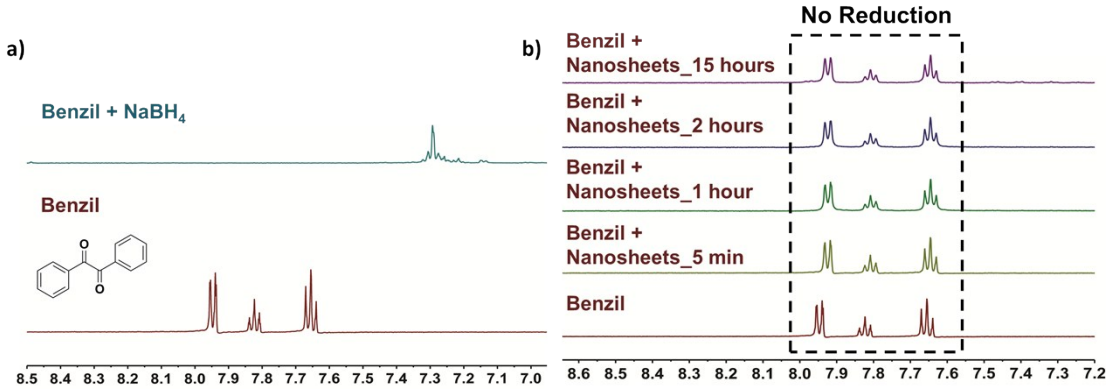

Figure S8: (a) Monitoring the $NaBH_4$ mediated reduction of benzil by ^1H solution NMR spectroscopy shows that $NaBH_4$ is capable of reducing benzil; (b) After addition of the nanosheets into benzil, there is no change in the NMR spectra, even after 15 hours, thereby showing that the nanosheets are unable to reduce the compound.

The standard reduction potentials of the tested compounds have been presented in Figure 2a in the main article file to identify the range of molecules that can be reduced by the nanosheets.[6,7,8]

S2.2. Gold Nanoparticle Decorated Boron-based Nanosheets

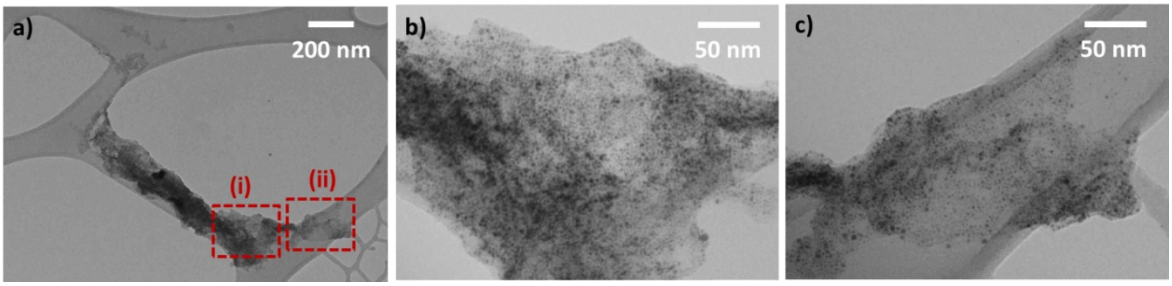

Figure S9: Low magnification TEM images depicting dense decoration of boron based nanosheets with nanoparticles: (a) Nanosheet on a lacey carbon grid; (b,c) Magnified images of the regions (i and ii) showing areas densely covered with nanoparticles.

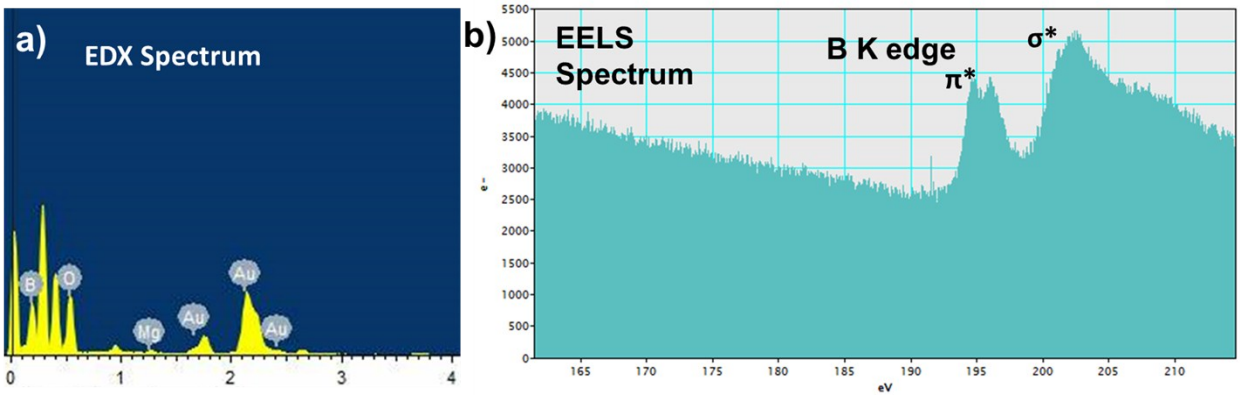

Figure S10: (a) EDX spectrum showing the presence of Au and B, in addition to Mg and O; (b) The EELS spectrum shows edges in the region between 190-205 eV, indicating it is indeed a boron based structure. The edges around 195 eV and 203 eV correspond to transitions from 1s to π* and σ* orbitals respectively.

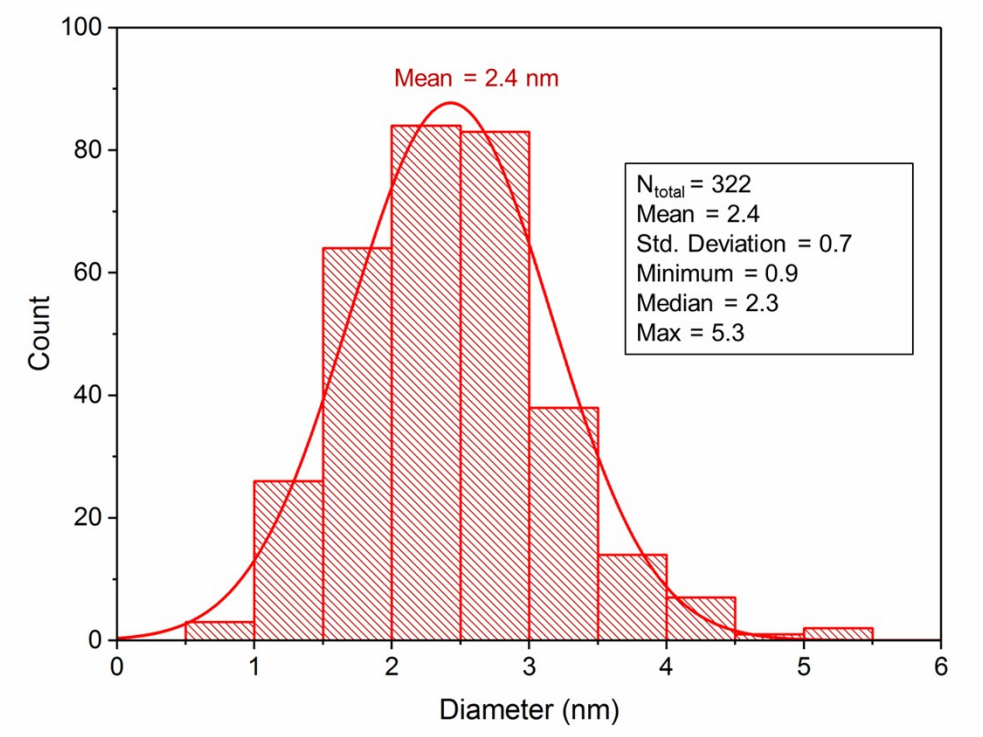

Figure S11: Size distribution of the nanoparticles formed by the reducing action of nanosheets: Histogram indicating that the formed nanoparticles are typically less than 10 nm in size, with the mean size ~2.4 nm. The HRTEM images of gold nanoparticle-nanosheet hybrids were analyzed using ImageJ software. The particle size histogram was plotted and the data was fitted to normal distribution using Origin Pro 2017 Graphing and Analysis software. Descriptive statistics obtained from the above data are presented in the inset.

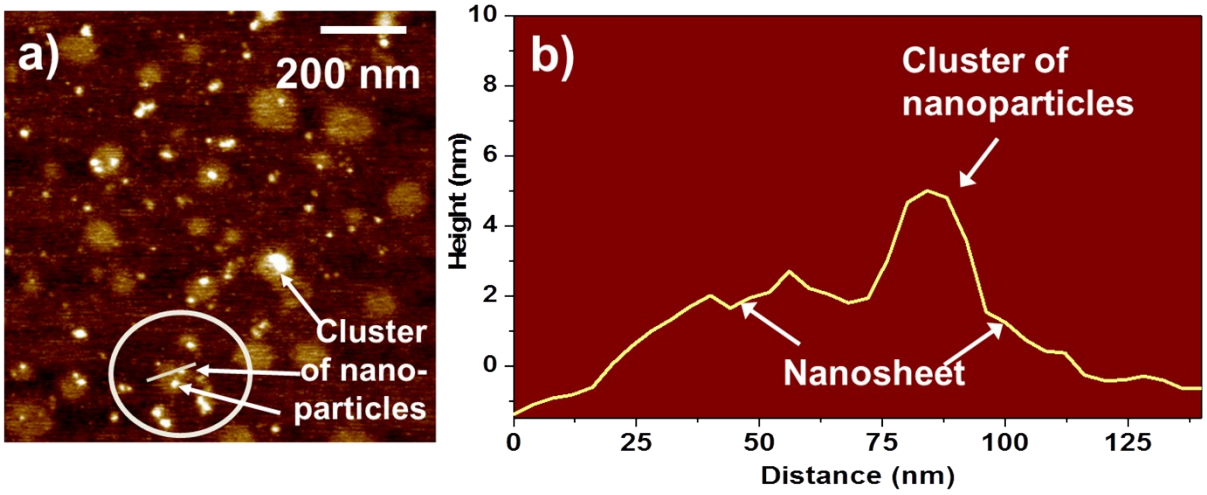

Figure S12: AFM image of AuNP-nanosheet hybrid: (a) AFM image shows clusters of nanoparticles present on nanosheets; (b) The height profile corresponding to the structure in a) marked with a circle.

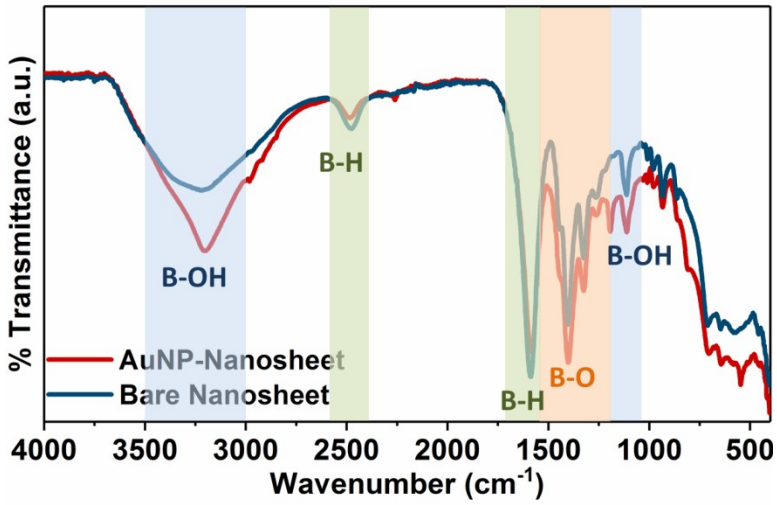

Figure S13: Comparing FTIR spectra of the bare boron based nanosheets and gold nanoparticle decorated nanosheets. The intensity of the B-H bands has decreased in the nanohybrids, whereas the intensity of the B-O and B-OH bands have increased when compared with the bare nanosheets.

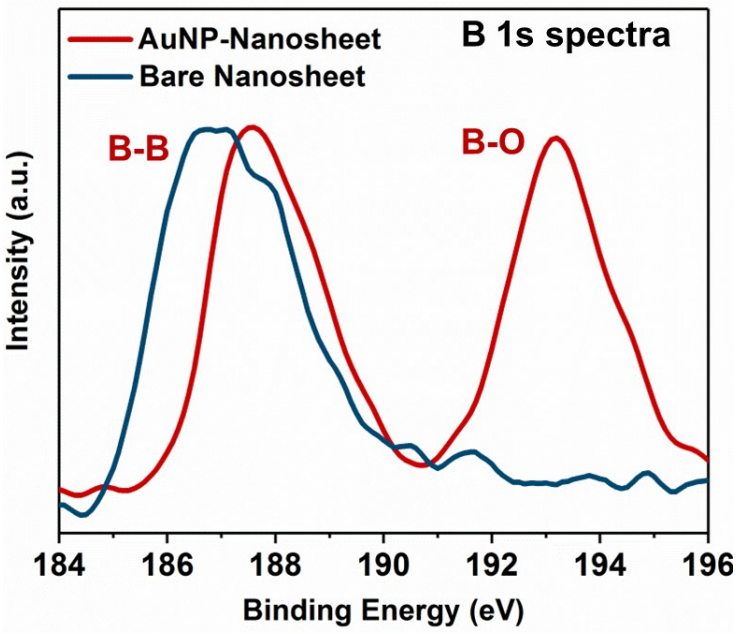

Figure S14: B 1s spectra acquired from the XPS analysis of the bare nanosheets and the AuNP-nanohybrid samples:

The B1s spectrum acquired from the bare nanosheets has a major peak ~186-188 eV which is characteristic of boron-boron coordination in metal borides.[9] The nanohybrids sample, on the other hand, displays two main peaks corresponding to two chemical states manifested by B atoms. The peak around 187.6 eV which corresponds to B-B, reflects a shift to higher binding energies when compared to the primary peak in the nanosheets. We expect this shift to stem from the fact that in the nanohybrids, the boron atoms now exist around a more electronegative Au species. Apart from this, a new peak centered ~193.2 eV has emerged in the nanohybrids sample, which corresponds to an oxidized form of boron, mainly as boron oxide B_2O_3.[10]

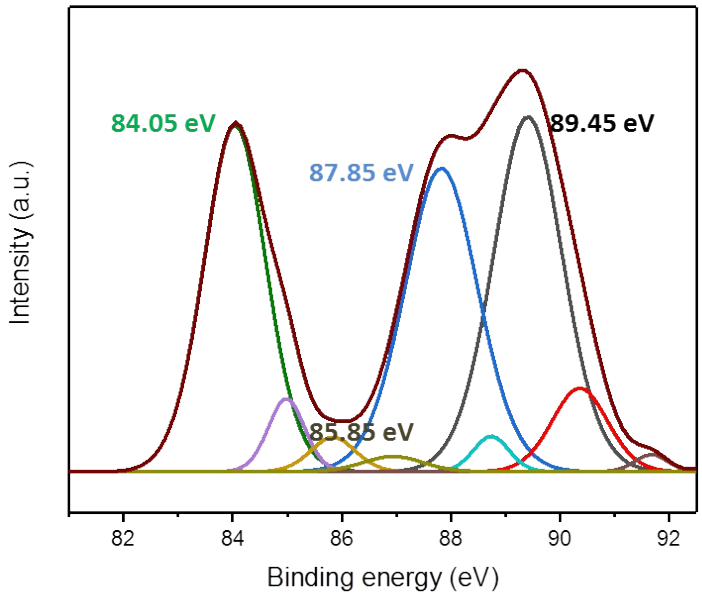

Figure S15: Au 4f spectra acquired from the nanohybrid sample

The Au 4f spectrum is depicted with the 4f $_{7/2}$ and 4f $_{5/2}$ doublets. The deconvoluted spectra are also shown. Upon deconvolution, many daughter peaks are seen, with the most intense peaks being located at binding energies of 84.05 eV, 87.85 eV, and 89.45 eV. The peaks at 84.05 eV and 87.85 eV can be attributed to Au^0 present in the inner core of the AuNPs. The peaks at higher energies may be assigned to the Au atoms on the surface of the AuNPs which are expected to interact with the nanosheets and are hence involved in Au-nanosheet binding. The other minor peaks could correspond to ionized Au species existing in valence states between Au^0 and Au^{3+}, which are present in the AuNP-Nanosheet interface. The origin of certain peaks like the one at 89.45 eV is unclear. We suspect charging effects to be one reason that contributes to such a peak at higher binding energies.

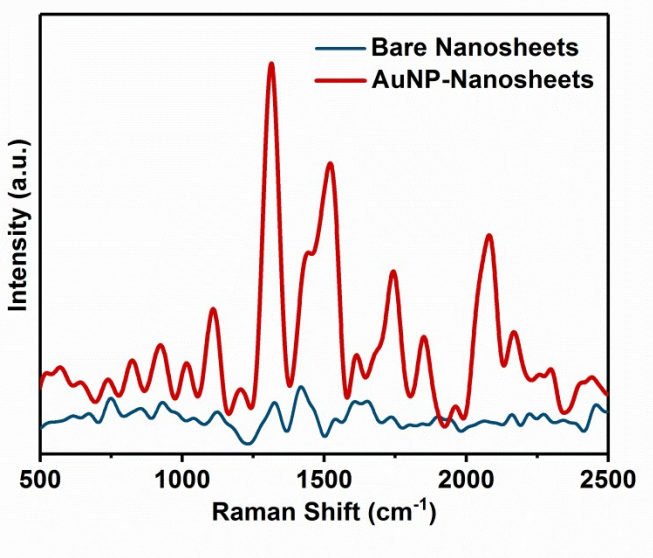

Figure S16: Comparing the Raman spectra of the bare nanosheets and the nanohybrids reveals that the nanohybrids exhibit a Raman signal enhanced by ~16 times, which suggests a chemical interaction between nanosheets and the gold nanoparticles

Upon conjugation of gold nanoparticles onto the nanosheets, the intensity of the Raman signal has increased which is attributed to surface enhanced Raman scattering (SERS). Such an enhancement can be because of two mechanisms: (i) electromagnetic - wherein the enhancement (by 10^4-10^6 factors) is caused by excitation of electromagnetic resonances (metal roughness/ particle sizes ~ 100 nm), (ii) chemical - wherein enhancement (by ~10^2 factor) is due to new electronic excitations (charge transfer possibly) in the adsorbed molecules leading to resonance Raman scattering. Hence, the low factor of enhancement in Raman signal implies a chemical interaction between the gold nanoparticles and nanosheets.

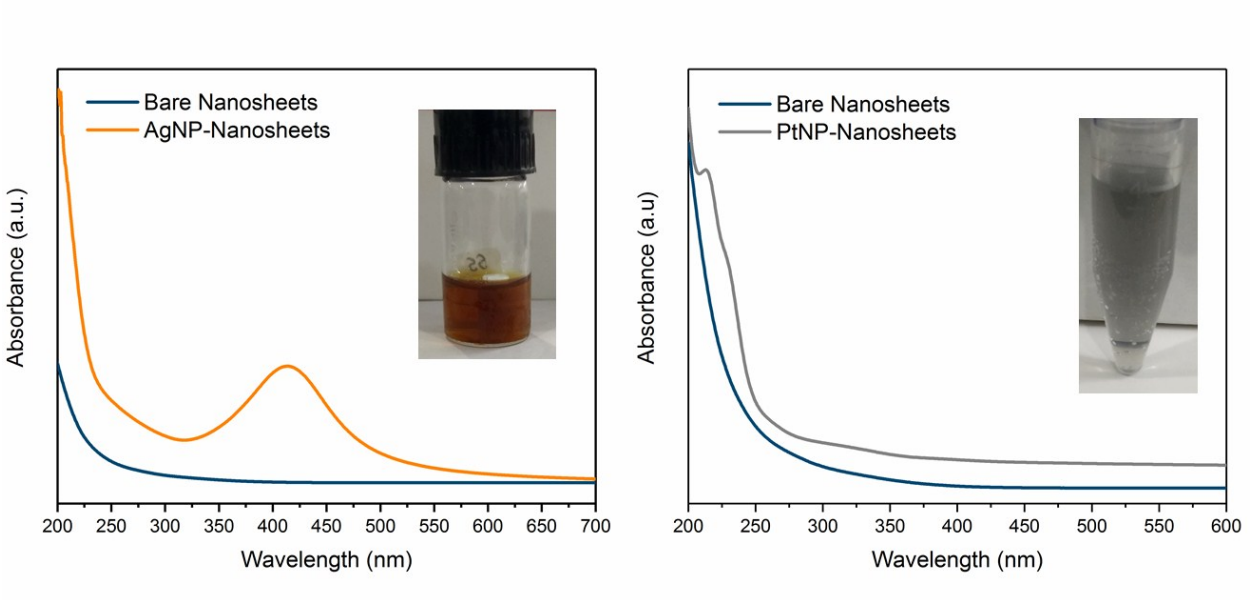

Figure S17: Comparing the UV Vis spectra of the bare nanosheets and the metal nanoparticle hybrids: (a) the nanosheets enable the reduction of silver nitrate and forms silver nanoparticles as evident from the dark yellow colored solution; (b) the nanosheets also reduce chloroplatinic acid to form platinum nanoparticles as evidenced by the black color of the dispersion.

S2.3. Reduction of graphene oxide to form reduced graphene oxide-boron based nanosheets hybrids

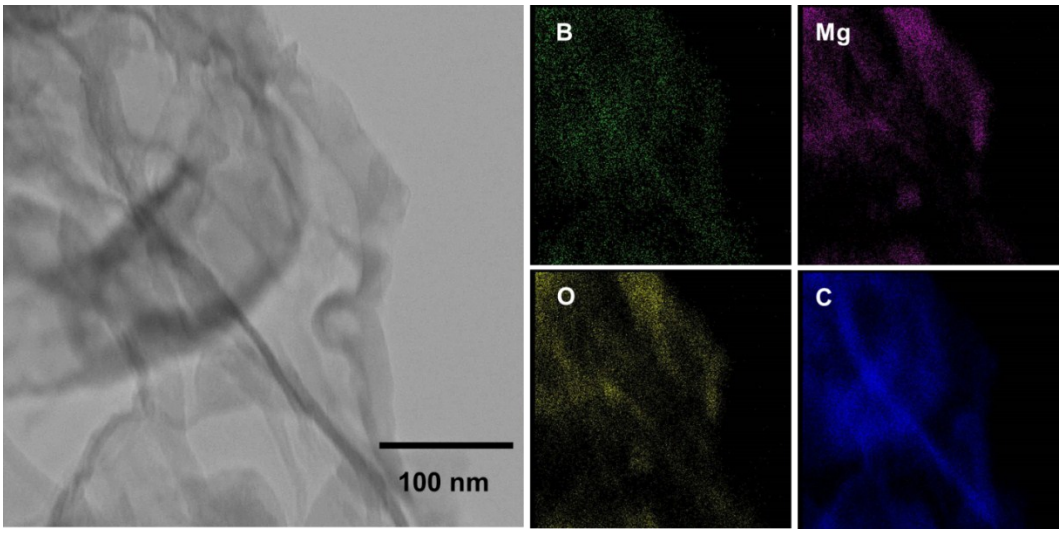

Figure S18: STEM-Elemental mapping of rGO-Boron based nanosheet hybrids show the presence of B and Mg in addition to C and Mg. It may be noted that detecting boron is difficult under EDX as it is a low atomic weight element. Therefore the presence of residual Mg on the boron based nanosheets could be used as an indication of their presence on the hybrids as well.

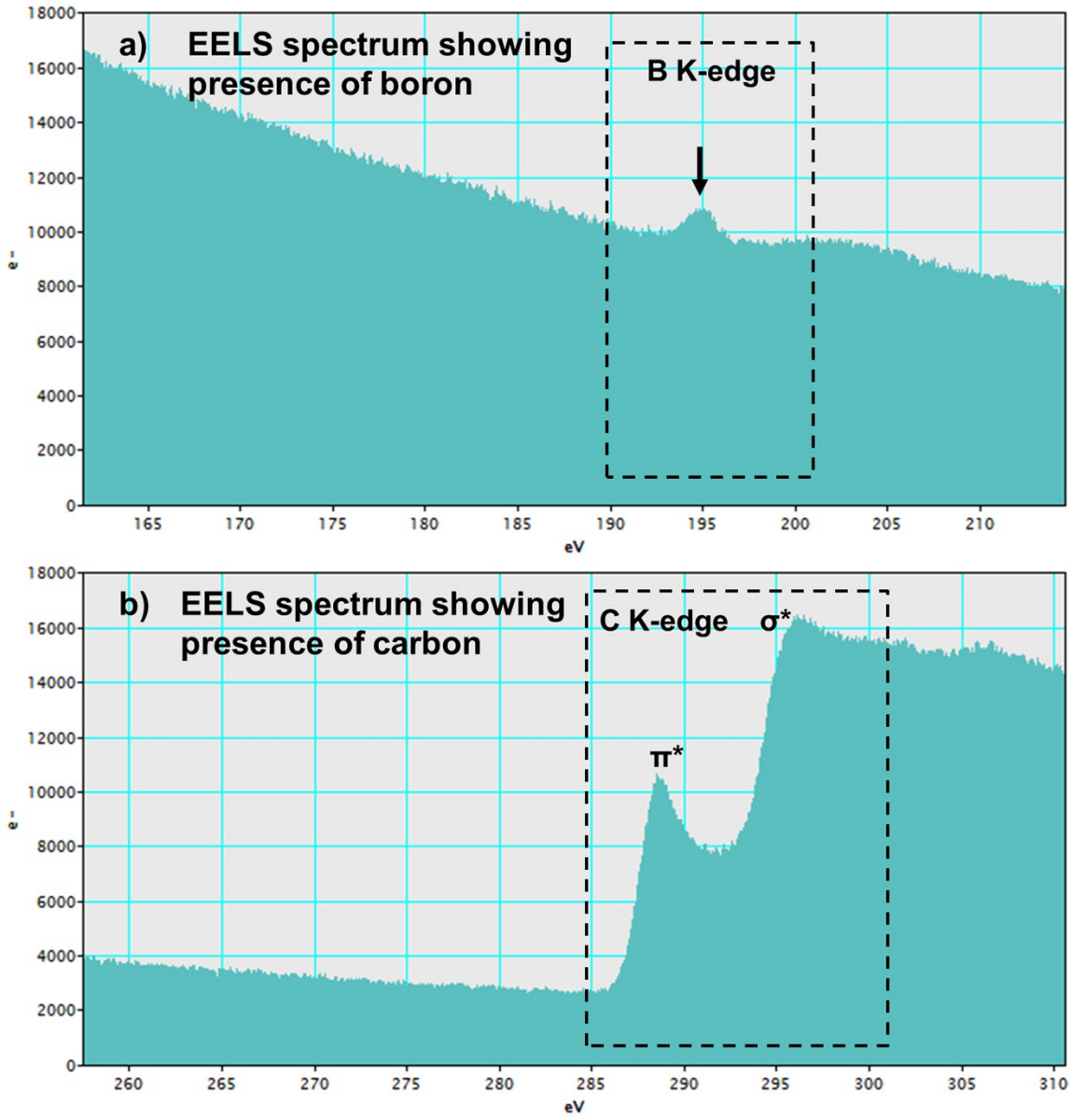

Figure S19: EELS of rGO-Boron based nanosheet hybrids show the presence of boron and carbon. The boron edge is of low intensity because it is difficult to detect boron when it is present together with carbon. The C K edge spectrum shows σ to π* and σ to σ* transitions.

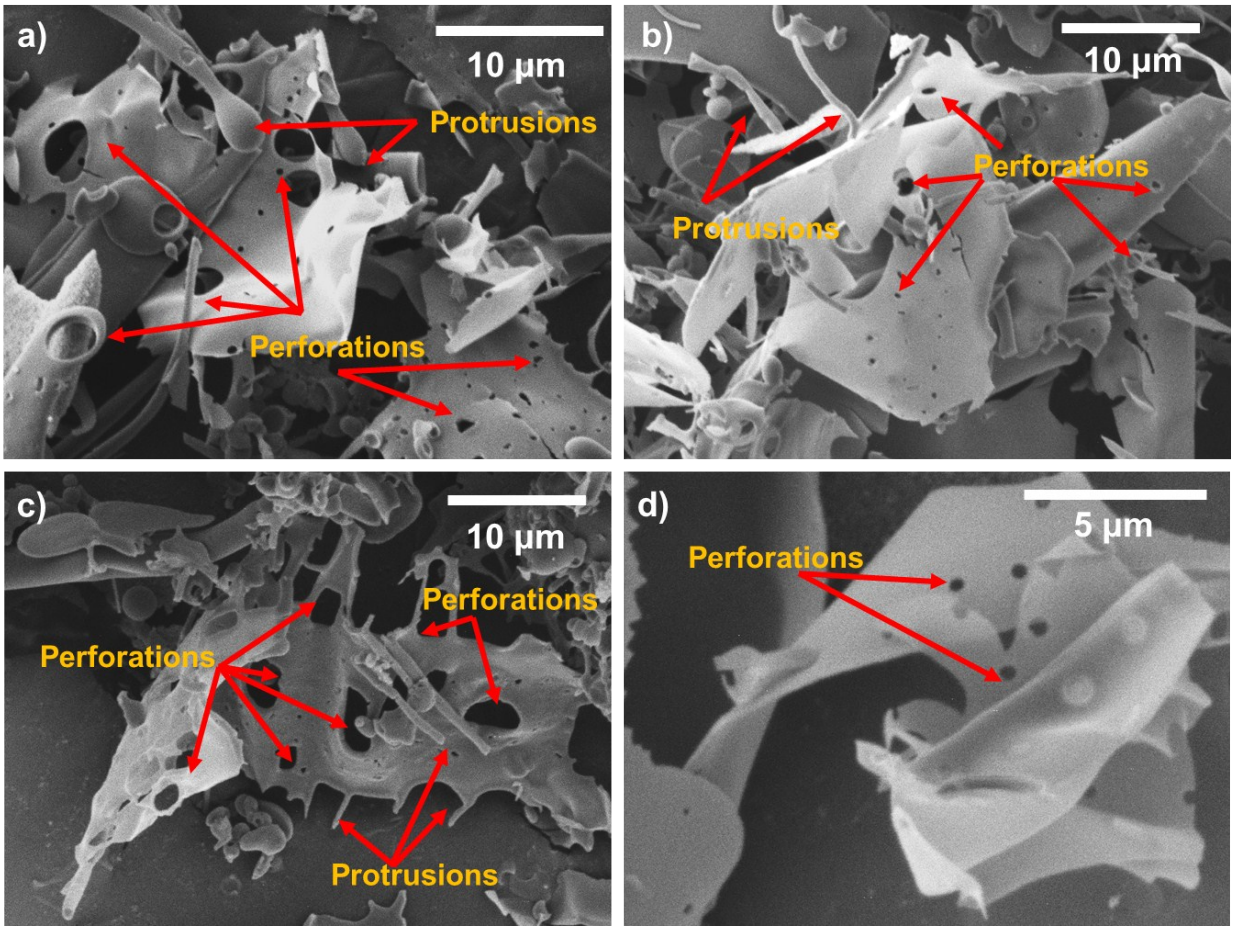

Figure S20: FE-SEM images of boron based nanosheets displaying characteristic perforations and spherical and rod-like protrusions

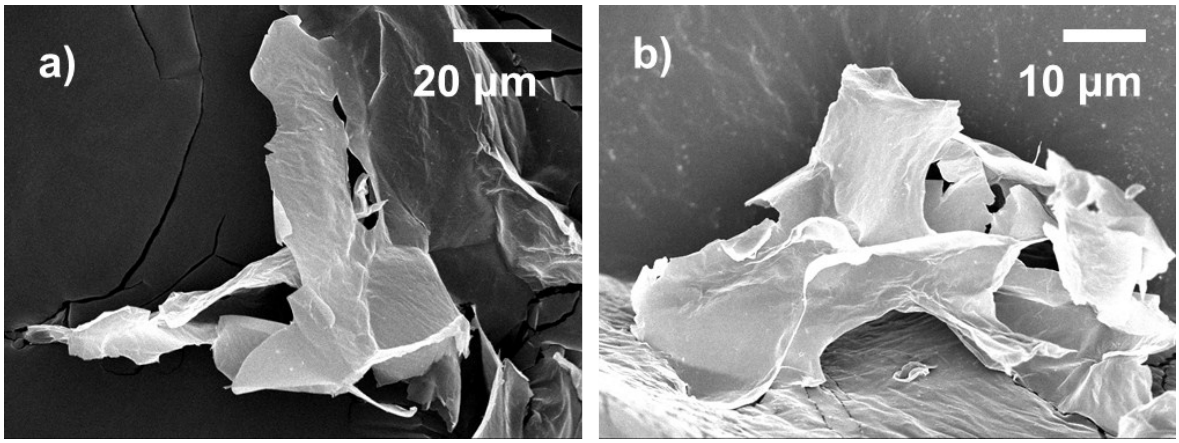

Figure S21: FE-SEM images of Graphene oxide (GO) nanosheets, wherein they are seen as thin flakes, with folded edges

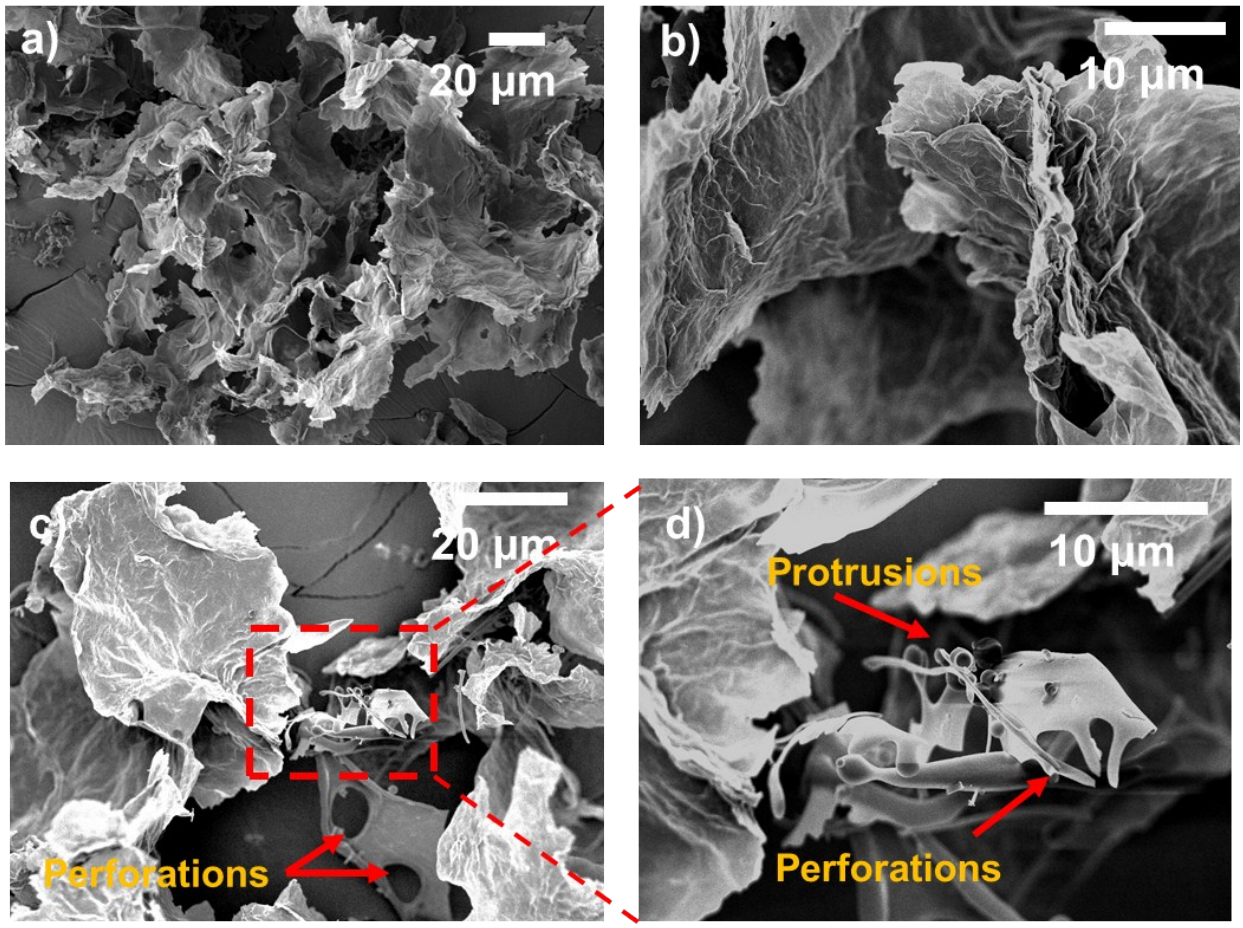

Figure S22: FE-SEM images of the hybrid structures formed as GO gets reduced by boron based nanosheets. These are wrinkled and show the presence of large perforations as well as structures typical of the boron based nanosheets (rod-like and spherical protrusions) indicating that a rGO-boron based nanohybrid has indeed formed.

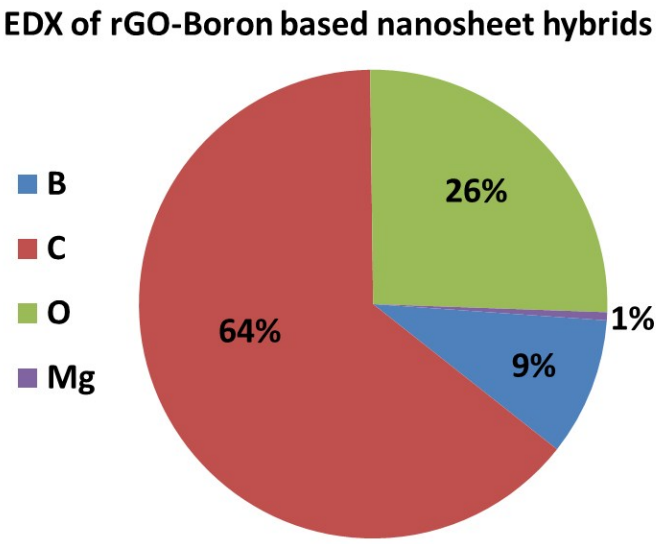

Figure S23: EDX Analysis: The nanohybrids have an elemental composition consisting of mainly C and O in addition to lower atomic% of B and Mg. The residual Mg in the boron based nanosheets is from the chemical exfoliation of MgB_2.

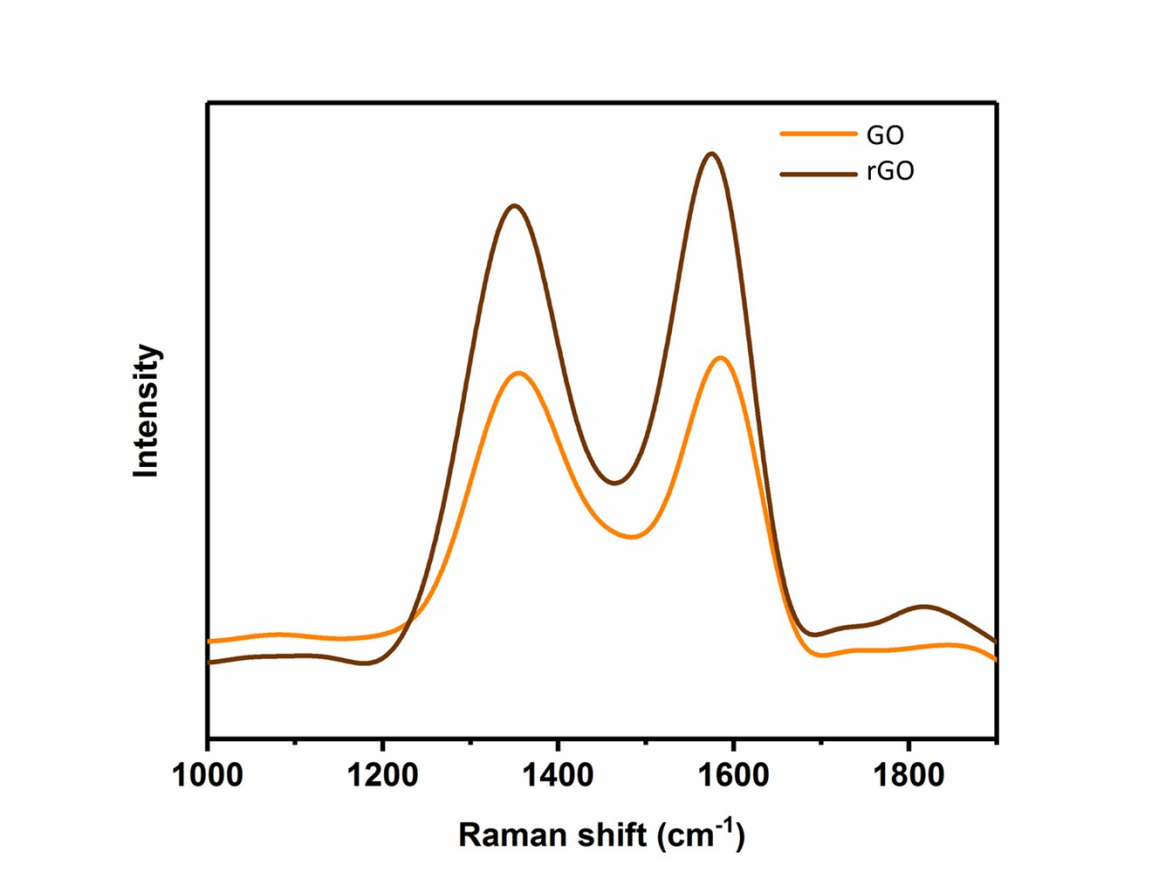

Figure S24: Raman spectra of rGO-boron based nanosheet hybrids compared with GO nanosheets, show the characteristic D and G bands. The G band corresponds to the in-plane stretching of sp^2 carbon atoms and gives an idea about the degree of graphitization. The D band being associated with structural defects and disorder in the carbon lattice. The D and G bands of rGO-boron hybrids are found to be ~1350 and 1575 cm^{-1}, whereas for GO sample these are at 1354 and 1584 cm^{-1}. The ratio between the intensity of D band to that of the G band (I_D/I_G) is used to denote the relative disorder in graphenic structures. I_D/I_G of GO was found to be 0.953, indicative of disorder in the graphitic structure due to the presence of oxygen groups. The I_D/I_G of rGO hybrids was found to be 0.902, which reflects a partial restoration of sp^2 domains due to the removal of oxy groups by virtue of reduction by the boron based nanosheets. Such incidences of reduced I_D/I_G by virtue of structural changes induced by reduction using chemical reagents like $NaBH_4$ and $LiAlH_4$ have been reported previously.[11]

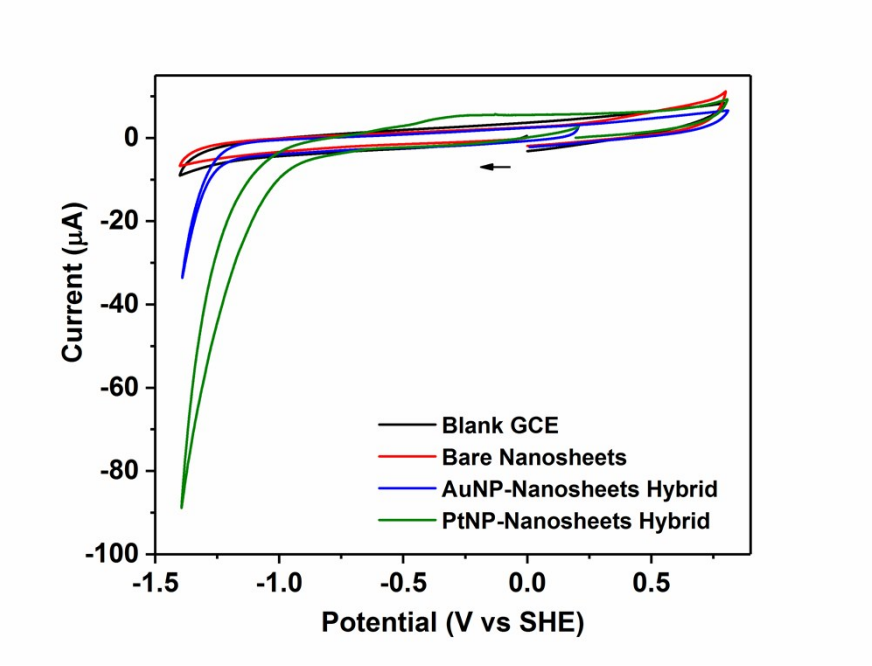

Figure S25: Cyclic voltammograms depicting the electrochemical response for hydrogen evolution reaction obtained from – bare electrode (blank glassy carbon electrode), electrode coated with boron based nanosheets, electrode coated with gold nanoparticle-nanosheet hybrids, and electrode coated with platinum nanoparticle-nanosheet hybrids in a neutral medium (pH 7.4, PBS buffer).

The presence of boron-metal interfaces motivated us to investigate the potential of boron based nanosheets and their metal nanoparticle hybrids for electrochemical hydrogen evolution reaction (HER). We carried out the electrocatalytic experiments by comparing the response of glassy carbon electrodes (GCE) with and without the nanomaterial. While the bare boron based nanosheets did not exhibit any electrocatalytic activity towards HER, the AuNP-nanosheets hybrids and PtNP-nanosheets hybrids showed a considerable H_2 production. The onset potential values for AuNP-nanosheets hybrids and PtNP-nanosheets hybrids were found to be -1.18 V (vs SHE) and -0.87 V (vs SHE), respectively. Thus at pH 7.4 (where equilibrium potential for H^+ reduction i.e. $E_{H+/0.5H2}$ is 7.4 X -0.059 V= -0.436 V vs. SHE), the overpotential requirement for AuNP-nanosheets hybrids is 744 mV, and for PtNP-nanosheets hybrids it is 434 mV. (The overpotential requirement is the difference between the potential where a particular reaction is occuring and its equlibrium potential). Furthermore, the HER catalytic current (measured at -1.4 V) was found to be ~2.7 times higher for PtNP-nanosheets hybrids when compared with AuNP-nanosheets hybrids. The bare glassy carbon electrode was scanned similarly to ensure that there was no HER activity inherently from the electrode itself under the experimental conditions. We inferred that the catalytic potential of the bare nanosheets is limited probably because of their non-conductive nature

which is attributed to a high degree of functionalization[1] as well as huge overpotential associated with poor bonding with H^+ or other intermediates during the formation of H_2. On the other hand, once they are decorated with the conductive metallic nanoparticles, this limitation is overcome. The nanosheets decorated with nanoparticles are expected to have enhanced potential for catalysis due to an increased number of active sites, and the synergy between nanoparticles and nanosheets. In the near future, we aim to explore how the constitution of nanoparticles and their loading capacity onto the nanosheets can influence the HER in aqueous solution at different pH conditions.

References

1. A. L. James and K. Jasuja, *RSC Advances*, 2017, **7**, 1905-1914.
2. O. C. Compton, S. W. Cranford, K. W. Putz, Z. An, L. C. Brinson, M. J. Buehler and S. T. Nguyen, *ACS Nano*, 2012, **6**, 2008-2019.
3. T. A. Prikhna, *Journal*, 2009, **0912**, 4906.
4. F. Zhao, X. Xing, C. Xiao, R. Hu, L. Xue, H. Gao, L. Xiao and T. An, *American Journal of Analytical Chemistry*, 2011, **2**, 270.
5. A. Remhof, Y. Yan, D. Rentsch, A. Borgschulte, C. M. Jensen and A. Zuttel, *Journal of Materials Chemistry A*, 2014, **2**, 7244-7249.
6. J. B. Conant and L. F. Fieser, *Journal of the American Chemical Society*, 1924, **46**, 1858-1881.
7. S. Jovanovic, K. Konya and J. Scaiano, *Can. J. Chem.*, 1995, **73**, 1803-1810.
8. H. E. Stapelfeldt and S. P. Perone, *Anal. Chem.*, 1969, **41**, 623-627.
9. R. P. Vasquez, C. U. Jung, M.-S. Park, H.-J. Kim, J. Y. Kim and S.-I. Lee, *Physical Review B*, 2001, **64**, 052510.
10. K. B. Garg, T. Chatterji, S. Dalela, M. Heinonnen, J. Leiro, B. Dalela and R. K. Singhal, *Solid State Communications*, 2004, **131**, 343-347.
11. A. Ambrosi, C. K. Chua, A. Bonanni and M. Pumera, *Chem. Mater.*, 2012, **24**, 2292-2298.